J Fluoresc (2012) 22:1617–1625
DOI 10.1007/s10895-012-1105-6

ORIGINAL PAPER

A Novel Reconfigurable Optical Biosensor Based on DNA Aptamers and a DNA Molecular Beacon

Chittanon Buranachai · Panote Thavarungkul · Proespichaya Kanatharana

Received: 21 May 2012 / Accepted: 27 June 2012 / Published online: 19 July 2012

Abstract In order to alter a typical molecular aptamer beacon (MAB) to detect a different analyte there is currently a need to change the whole sensor unit including the expensive labeling fluorophores. In this work a DNA-based reconfigurable molecular aptamer beacon was developed. It is composed of two parts: a variable part and a constant part. The variable part comprises an aptamer strand and its complementary strand while the constant part is an oligonucleotide doubly labeled with a Förster Resonance Energy Transfer (FRET) pair and the two parts become joined via DNA hybridization. The sensor exists in two conformations: a folded (high FRET) and an unfolded (low FRET) in the absence and presence of the aptamer-target binding respectively. This sensor can be reconfigured by washing away the aptamer and the complementary strand using proper complementary strands, called washers. As a proof of the principle, a sensor that bound the enzyme thrombin, an analyte with a strong binding, was first constructed and then reconfigured to bind adenosine, selected as an analyte with a weak binding. We believe that the design is of universal use applicable to many types of aptamers.

Keywords Optical biosensor · DNA nano-device · FRET · Aptamers

Introduction

Sensors based on functional DNA have become more popular in the past decade [1]. One of the most fundamental building blocks of this type of sensor is an aptamer, which is a single stranded oligonucleotide capable of binding specifically to its target and is selected via the method of systematic evolution of ligands by exponential enrichment (SELEX) [2, 3]. Aptamers rival antibodies in many circumstances, such as when the working condition is hostile to protein [4]. There are several detection techniques utilizing the aptamer based sensors, such as electrochemical [5], mass sensitive [6], surface plasmon resonance [7], colorimetric and UV–vis spectroscopy especially via the aggregation of nanoparticles [8]. However, the method utilizing fluorescent dyes labeling still offers good sensitivity. Since an aptamer usually undergoes conformational change upon binding to its target [9], one can achieve a labeled aptamer sensor by putting fluorescent dyes at positions adjacent to or on the target binding site where the binding leads to changes in the dyes' microenvironment and, therefore, changes in their fluorescence quantum yield. Alternatively one could utilize the change in the dye rotational freedom that occurs on binding to its target resulting in a change in the fluorescence anisotropy [10]. Though a single label proved to be cost effective, often it required a tertiary structure of the aptamer and the nature of the aptamer-target binding to be known a priori [1]. Double labeling could be utilized to avoid such a complication. In some of the very first demonstrations, modified aptamers capable of forming open-closed structures were doubly labeled with a fluorescent dye and a quencher [11, 12]. Binding of the target drived structural

Electronic supplementary material The online version of this article (doi:10.1007/s10895-012-1105-6) contains supplementary material, which is available to authorized users.

C. Buranachai (✉) · P. Thavarungkul
Trace Analysis and Biosensor Research Center, Department of Physics, Faculty of Science, Prince of Songkla University, Hat Yai, Songkhla 90112, Thailand
e-mail: chittanon.buranachai@gmail.com

P. Kanatharana
Trace Analysis and Biosensor Research Center, Department of Chemistry, Faculty of Science, Prince of Songkla University, Hat Yai, Songkhla 90112, Thailand

changes. This in turn changed the proximity of the dye-quencher resulting in a change in the fluorescence intensity, similar to the way the original molecular beacon worked [13, 14]. These hybrid sensors, a.k.a. molecular aptamer beacons (MABs) [15], have been improved over time. For example, the introduction of the structure switching aptamer [16] led to a universal design applicable to virtually any type of aptamer without prior knowledge of its secondary or tertiary structure or the nature of the aptamer-target binding.

However, almost all MABs shared one drawback: the fluorescent dyes were covalently labeled. While this should not be a problem with a single target small scale detection, it can be problematic in the case of a multiple target large scale detection because labeling fluorescent dyes is laborious and expensive and it is cumbersome to do every time for detecting a new target. Several groups have been trying to overcome this issue by using the "label free" method either by dye displacement essays [17] or by using a double aptamer in which one aptamer worked as a receptor to a target of interest and the other worked as a reporter binding to the signaling fluorophore malachite green [18].

Here we present an alternative and economical DNA MAB consisting of three oligonucleotides (Fig. 1). One is a base (B strand) doubly labeled with a FRET (Förster Resonance Energy Transfer) pair. The second is an aptamer (A strand, exemplified as tA and aA strands in the figure) and the third is a complementary strand to the aptamer (C strand, exemplified as tC and aC strands). The A and C strands are specific to a given target but are replaceable and the B strand is designed to be unchanged. Therefore, the sensor structure is similar to an antibody where a variable domain (consisted of A and C strands) is joined to a constant domain (B strand). This approach is economical because the expensive B strand can be used with many types of aptamer. Moreover, using a FRET pair provides an internal reference to the measured signal and having no RNA as a reporter could make the sensor more robust. Once annealed, the sensor exists in two conformations: folded and unfolded (Fig. 1a). In the absence of the target, the folded conformation is more favored via the formation of a double stranded domain between the A and C strands (domains 2:2* or 6:6* in Fig. 1b). In the presence of the target, however; the sticky ends hybridization gives way to the formation of an aptamer-target binding, destabilizing the folded conformation. In terms of FRET, the folded and unfolded conformations correspond to a high FRET and a low FRET state. The design is of universal use and it can be configured to detect different targets. To prove our concept, a thrombin sensor and an adenosine sensor were constructed using the described principle. Also, we demonstrate a step-by-step reconfiguration where the variable domain of the thrombin sensor (the tA and tC strands) can be removed and that of the adenosine sensor (the aA and aC strands) can be assembled onto the bare B strand.

Experimental Section

Materials

DNA Constructs All oligonucleotides were purchased from Integrated DNA Technology (IDTDNA, Coralville, IA, USA). Shown in Fig. 1b are the DNA sequences and names: the base (B strand) is a 40-mer labeled on the 5′ end with fluorescein (F) and on the 3′ end with tetramethylrhodamine (TMR). At the top of the figure, the anti-thrombin aptamer strand (tA strand) is a 30-mer designed to hybridize to the B strand creating a 12 base long double stranded domain (domain 3:3*) to ensure the stability during working conditions. The rest of the tA strand contains the canonical 15-base anti-thrombin aptamer sequence [20]. The anti-thrombin aptamer complementary strand (tC strand) has various lengths from 17 to 20 bases extending in the 3′ direction in domain 2*. Twelve bases of the tC strand hybridize to the B strand (domain 4:4*) while the rest is the sticky bases complementary to the anti-thrombin aptamer in the tA strand (domain 2:2*) overlapping the thrombin binding region. At the bottom of the figure, the anti-adenosine aptamer strand (aA strand) is a 39-mer and the anti-adenosine aptamer complementary strand (aC strand) is a 20-mer. Similar to the case of the tA and tC strands, both the aA and aC strands form a 12-base double stranded region with the B strand (domains 3:3* and 4:4*, respectively) and a sticky region to each other (domain 6:6*). The labeled oligos were purified by reverse phase HPLC as a standard procedure of the manufacturer and the unlabeled oligos were desalted. No further treatments were performed prior to use. The design of the oligos was done heuristically with the aid of UNAFold [21] (available at http://mfold.rna.albany.edu/) to verify the stability of hybridization under working conditions and to minimize any unintended secondary structures.

Thrombin Thrombin from human plasma was purchased from Sigma (T6884 Sigma Aldrich, St Louis, MO, USA). The concentration of thrombin was calculated by measuring the OD_{280} and using $E_{280}^{1\%} = 18.3$ provided by the manufacturer. The protein was stored in 0.1 %w/v BSA (B4284 Sigma Aldrich, St Louis, MO, USA) in 10 mM Tris pH 8.0, and kept as 200 μL aliquots at −20 °C for long term storage. For each measurement, the thrombin solution was

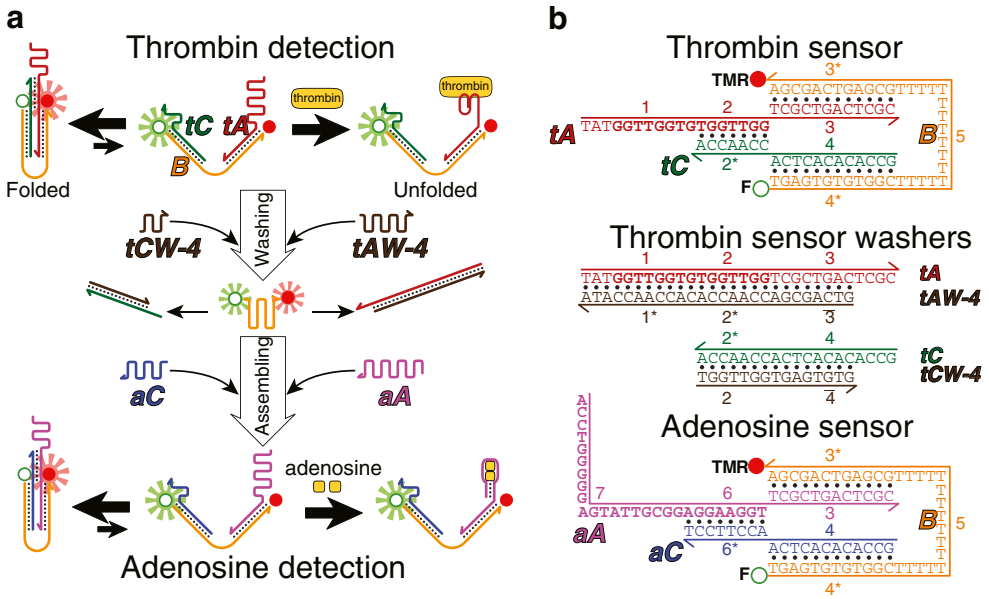

Fig. 1 **a** The operation principle of the reconfigurable molecular aptamer beacon sensor. On the top of the panel shows a thrombin sensor constructed from the B strand doubly labeled with fluorescein (F: *open circle*) and tetramethylrhodamine (TMR: *filled circle*) as a FRET pair, an anti-thrombin aptamer strand (tA strand) and an anti-thrombin aptamer complementary strand (tC strand). In the absence of thrombin, the folded structure (high FRET state) is more stable via the sticky ends hybridization but binding to thrombin causes the structure to unfold (low FRET state). The middle of the panel shows the reconfiguration; first an anti-thrombin aptamer washer (tAW-4 strand) and an anti-thrombin aptamer complementary washer (tCW-4 strand) are added to remove the tA and tC strands via strand displacement. Then, in the bottom of the panel, an anti-adenosine aptamer strand (aA strand) and an anti-adenosine aptamer complementary strand (aC strand) are added to assemble an adenosine sensor. The annealed sensor can detect adenosine following the same mechanism as in the case of the thrombin sensor. **b** The names and sequences of oligomers used in this study. The bold fonts mark the aptamer sequences. Following a popular practice in DNA nanotechnology [19], oligos are depicted as directional lines with the hook marking the 3′ end. The sensors are divided into domains, each represented by a number. In our design, a domain is fully complementary to the starred domain but partially complementary to the barred domain. For example domain 3 on the tA strand (on the top of the panel) is fully complementary to domain 3* on the B strand but partially complementary to domain 3 on the washer strand (tAW-4, in the middle of the panel). A double stranded domain is represented by two numbers joined by a colon, e.g. 3:3*. The key domains of the sensors are domain 2 and 6, which are a part of the thrombin and the adenosine aptamer, respectively. They can hybridize with domain 2* and 6* in the absence of target but are hidden when the aptamers fold upon target binding. The tAW-4 and tCW-4 washers contain domain 3 and 4 (instead of domain 3* and 4*) to reduce the unintended hybridizations of the washers to the aA and aC strands to be mixed in in the assembling step

thawed and mixed well prior to use. Each aliquot was used only within 5 days after thawing.

Adenosine Adenosine was purchased from Sigma (A9251 Sigma Aldrich, St Louis, USA). The concentration was calculated by using ε_{259}=15,400 M^{-1} cm^{-1} [22].

Sensor Preparation

Stock solutions of oligos were made by diluting lyophilized DNA powder in DI water. The concentrations of the stock solution of unlabeled oligos were obtained by measuring the OD_{260} using the extinction coefficient values provided by the manufacturer. The concentration of the stock solution of the doubly labeled oligos were calculated from the measured absorption of TMR at 558 nm (OD_{558}) using the extinction coefficient value of 75,200 M^{-1} cm^{-1} [23]. The stock solutions were then kept as 200 μL aliquots at −20 °C for long term storage. An annealed thrombin sensor was prepared by mixing the B, tA and tC strands at the desired ratio in the presence of 200 mM NaCl in 10 mM Tris pH 8.0. For the 1:1:1 (B:tA:tC) strand mixing ratio, 15 μM of each was used and scaled up accordingly for the higher mixing ratio. The mixture was incubated at 90 °C for 10 min in a water bath and left to cool down to room temperature overnight. An annealed adenosine sensor was prepared by the same method.

FRET Measurement and Analysis

The $(Ratio)_A$ Measurement The conformational changes of the sensor were followed by measurement of the Förster Resonance Energy Transfer (FRET) efficiency. In this work we measured FRET efficiency E indirectly by measuring sensitized acceptor fluorescence via the $(ratio)_A$ method [24]. Selecting fluorescein and tetramethylrhodamine

excitation wavelengths near their absorption maxima at 495 nm and 550 nm respectively, the $(\text{ratio})_A$ is related to E as follows:

$$(\text{ratio})_A = \frac{\gamma}{\gamma+\beta} \times \frac{\varepsilon_F(495) \times E + \varepsilon_{TMR}(495)}{\varepsilon_{TMR}(550)} \quad (1)$$

Where

- γ is the fraction of sensors with a complete donor-acceptor labeling
- β is the fraction of sensors singly labeled with only acceptor

$\varepsilon_F(495)$, $\varepsilon_{TMR}(495)$ and $\varepsilon_{TMR}(550)$ are the extinction coefficients of fluorescein at 495 nm, of tetramethylrhodamine at 495 nm and at 550 nm, respectively.

Alternatively, the $(\text{ratio})_A$ can be taken as a ratio between the TMR total emission intensity being excited at 495 nm (via the effect of FRET combined with that of direct excitation) and the TMR total emission intensity being excited at 550 nm (via the effect of direct excitation alone), as shown in Eq. 2 (adapted from [25]).

$$(\text{ratio})_A = \frac{\sum_i F_{TMR}(\lambda_{495}, \lambda_i)}{\sum_i F_{TMR}(\lambda_{550}, \lambda_i)} \quad (2)$$

Therefore, the $(\text{ratio})_A$ is measured by first taking an emission spectrum with an excitation wavelength at 495 nm and removing the contribution of the donor emission using a known fluorescein emission spectrum. Then the second emission spectrum is obtained by a 550 nm excitation. The $(\text{ratio})_A$ is the ratio of the spectral area of the two spectra. (See Figure 6 in the Supplementary information for more details.)

All emission spectra were measured on a Perkin Elmer LS55 spectrofluorometer (Perkin Elmer Inc., Waltham, MA, USA). To ensure that the measured emission signal represented the total fluorescence intensity, an excitation and an emission polarizer were employed during the measurement. For a given measurement, the excitation light was maintained vertically polarized by the excitation polarizer, while two emission spectra were collected: one with the vertical emission polarizer and the other with the horizontal emission polarizer. The two obtained spectra were denoted $F_{VV}(\lambda_{ex}, \lambda)$ and $F_{VH}(\lambda_{ex}, \lambda)$. The spectrum representing the total fluorescence intensity $F_{total}(\lambda_{ex}, \lambda)$ was constructed by calculating the total fluorescence intensity at each emitted wavelength λ_i using [26].

$$F_{total}(\lambda_{ex}, \lambda_i) = F_{VV}(\lambda_{ex}, \lambda_i) + 2 \times G(\lambda_i) \times F_{VH}(\lambda_{ex}, \lambda_i) \quad (3)$$

Where $G(\lambda_i)$ is the G factor at a given λ_i obtained from $G(\lambda_i) = \frac{F_{HV}(\lambda_{ex}, \lambda_i)}{F_{HH}(\lambda_{ex}, \lambda_i)}$

Thrombin and Adenosine Titration The annealed thrombin sensor (designated tC-B-tA) or the annealed adenosine sensor (designated aC-B-aA) was diluted from the annealing stock with 10 mM Tris pH 8.0, mixed with $MgCl_2$ and KCl stock solutions and incubated in a micro-centrifuge tube in the dark at room temperature for 30 min. Thrombin or adenosine was then added and the incubation allowed to proceed for 1 h. Unless specified otherwise, the final mixture was 133 nM tC-B-tA (measured from the absorption of TMR at OD_{558}) in 0.1 %w/v BSA in 10 mM Tris pH 8.0 containing residual 1.77 mM NaCl used in annealing and various concentrations of $MgCl_2$, KCl and thrombin/adenosine. To preserve the samples, some, but not all, data points in each titration were measured three times. The obtained standard deviations were used to verify if the change in the $(\text{ratio})_A$ was significant.

Reconfiguration The experiment was divided into 6 separate steps: #1 starting with the annealed thrombin sensor, #2 washing of the tC strand, #3 washing of both the tC and tA strand from the B strand, #4 assembling of the aA strand on the B strand, #5 assembling of both the aA and the aC strand on the B strand creating a functioning adenosine sensor and #6 testing the sensor response with 20 μM adenosine. The $(\text{ratio})_A$ was measured for each of the six steps. For a practical reason, the sample preparation was carried out in 6 batches for the 6 reaction steps. The details of the preparation can be found in the Supplementary information.

Results and Discussion

Thrombin Sensor

The Effect of Mg^{2+} and K^+ Concentration

The performance of the sensor relies on a balance between a strong folded conformation in the absence of thrombin and an ease of transition to the unfolded conformation once thrombin binds. One would prefer a major fraction of the sensors to be in the folded structure prior to adding thrombin for a high initial FRET efficiency value but would rather have an efficient structural switching after thrombin binding for a big decrease in the FRET efficiency. The folded

conformation is stable in the presence of cationic species because of the metal ions-phosphate oxygen interaction stabilizing the sticky ends hybridization (domain 2:2*) while the unfolded conformation is likely to be stable in the presence of either K^+ or Na^+ because these two ions help with the strong formation of a G-quadruplex [27, 28] found in the anti-thrombin aptamer [29–31] (domain 1 and 2 combined). Mg^{2+} is chosen to stabilize the folded structure due to its superior efficiency compared with other mono and divalent cations [32] while having a much weaker effect on the G-quadruplex formation when compared with monovalent cations [33] and K^+ is chosen to ease the transition from the folded to the unfolded structure. In order to obtain the optimal performance, the concentrations of the two ions need to be optimized.

Figure 2 shows the results obtained from the $(ratio)_A$ method performed at different concentrations of Mg^{2+}, K^+ and thrombin. First the concentration of Mg^{2+} was varied from 5, 10, 20, 50 and 100 mM while the K^+ concentration was fixed at 5 mM. In Fig. 2a, at 100 mM $MgCl_2$ there was no significant change in the $(ratio)_A$ beyond the standard deviations with an increasing amount of thrombin. However, at the lower $MgCl_2$ concentrations, the general trend of the result shows a decrease in the $(ratio)_A$ upon increasing thrombin concentration. This follows the working principle of the sensor that thrombin binding disrupts the folded conformation (high FRET i.e. high $(ratio)_A$) making the sensor unfold (low FRET i.e. low $(ratio)_A$). However there are differences in two aspects: the initial $(ratio)_A$ and the sensitivity. The initial $(ratio)_A$ in the absence of thrombin increases with the increasing Mg^{2+} concentration. This agrees with our hypothesis mentioned above that the sticky ends hybridization is stable at high salt concentration. The sensitivity, defined as the absolute value of the slope, on the other hand is high at low $[Mg^{2+}]$ and tapers off with increasing $[Mg^{2+}]$. Since the sensitivity reflects how easily the folded structure can switch to the unfolded one, it can be deduced that Mg^{2+} counteracts the transition. Therefore, while adding Mg^{2+} has the desirable effect of stabilizing the folded conformation, too high a concentration prevents the conformational transition. The sensitivity is an important property of a sensor, therefore 5 mM was chosen as the working concentration for Mg^{2+}. Note that the detection range is in the early nanomolar range, which is comparable to the thrombin sensors previously reported [15, 16].

Then the concentration of K^+ was varied from 0, 5, 10, 20, 50 and 100 mM while the Mg^{2+}concentration was fixed at 5 mM. When compared with Fig. 2a, the results in Fig. 2b show a similar trend of the $(ratio)_A$ decrease with the increasing thrombin concentration. However, the initial $(ratio)_A$ in this case decreases with increasing $[K^+]$. This is likely due to the fact that K^+ facilitates the formation of the G-quadruplex structure in the overhang region of the tA strand (domain 1 and 2 combined), which in turn, disrupts the sticky ends hybridization (domain 2:2*) of the folded conformation. The sensitivities in the case of 5, 10, 25 and 50 mM are comparable but slightly decrease at 100 mM. This is due to the fact that the sensor needs to bind thrombin while it is in the folded conformation in order to cause the change in the $(ratio)_A$. It is likely that high concentration of K^+ induces G-quadruplex formation making the majority of sensors unfold even in the absence of thrombin as seen in some reports on using the thrombin binding aptamer (TBA) to detect K^+ [34]. At 0 mM K^+, while the initial $(ratio)_A$ is the highest, the sensivity is low. This also agrees with the notion that a G-quadruplex formation needs monovalent

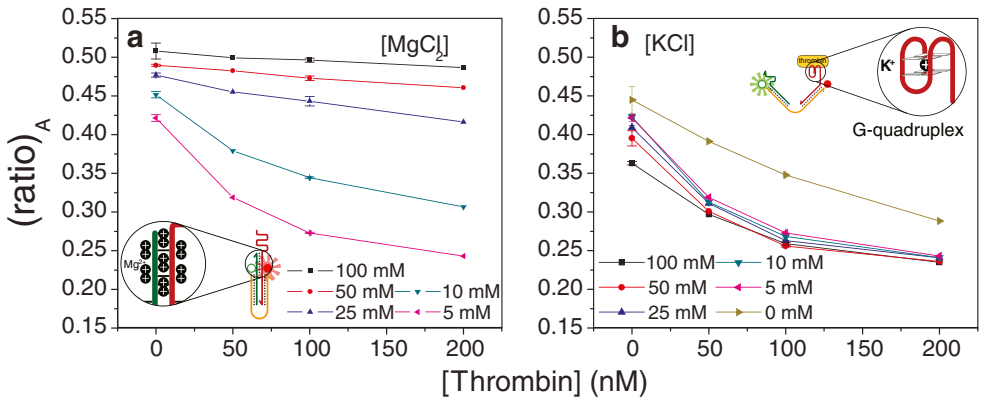

Fig. 2 The effect of Mg^{2+} (**a**) and K^+ (**b**) concentration on thrombin detection. The concentration of KCl was fixed at 5 mM in (**a**) and the concentration of $MgCl_2$ was fixed at 5 mM in (**b**). It is anticipated that Mg^{2+} ions stabilize the folded conformation by screening electrostatic repulsion between two phosphate backbones forming the sticky ends hybridization (domain 2:2*) (a, inset) while K^+ ions facilitate the G-quadruplex formation of the tA strand in domain 1 and 2 combined (b, inset) helping the transition to the unfolded structure upon thrombin binding. The strands ratio of 1:1:1 (B:tA:tC) was used in the sensor preparation step and the sticky base length was 7. Three independent measurements were done at 0 and 100 nM of thrombin concentrations for every graph shown in (**a**) and (**b**) with the error bars indicating the standard deviation

cations, K^+ and Na^+ in particular, as stabilizer; therefore it is difficult to switch to the unfolded structure in the absence of K^+. Note that at 0 mM K^+ the sensor still responds to thrombin possibly due to the background Na^+ (1.77 mM) used during the sensor preparation (see Experimental section for more details) and is still present after dilution or that thrombin itself helps to stabilize the G-quadruplex [35] or both effects combined. Focusing on the highest sensitivity, 5 mM was then chosen as the working concentration for K^+.

The Effect of Sticky end Length and the Effect of Strand Mixing Ratio

The sticky end length was varied to find the suitable strength of the folded structure. As already discussed, the sensitivity of the sensor depends on two contradicting effects: if the folded structure is too weak then the majority of the sensor will be in the unfolded conformation but if it is too strong it will resist the transition to the unfolded structure upon the binding of thrombin. In either case, the sensitivity will be compromised. The sensor is designed to have a portion of the aptamer sequence being able to form a double stranded domain via sticky ends hybridization so that the binding of an analyte competes with the hybridization. To study the suitable sticky end length, the tA strand was kept unchanged while the tC strand was varied in length from 17 to 20 bases extending in the 3′ direction corresponding to 5–8 bases long sticky end (domain 2*, shown as 7 bases long in Fig. 1b). As shown in Fig. 3a, the initial $(ratio)_A$ and the sensitivity both increased as the sticky base was extended from 5 to 7 bases. At 5-bases long the sticky end was too short for a stable folded structure so the majority of sensors started in the unfolded conformation, judged from the low $(ratio)_A$ and adding thrombin did not produce a significant change. Increasing the sticky base length to 6 and 7 bases improved the situation because more of the sensors favored the folded conformation and the binding with thrombin was more easily measurable. From the result it might be deduced that even though the 7-base sticky end provided good stability for the folded conformation, it was not too strong for an efficient transition to occur. Therefore, the sensitivity of 7-base long was more than that of 6-base long sticky end. Extending the sticky region to 8-base long did not significantly increase the initial $(ratio)_A$. However, the decrease of sensitivity at 8-base long is likely because the sticky end became stronger and was able to compete more effectively with the thrombin binding. As a result, the optimal length of the sticky end was set at 7 bases.

The effect of the molar ratio of the mixing strands was also tested by fixing the B strand at 15 μM in the annealing step while the tA and tC strands were varied according to the desired ratio. From the results presented in Fig. 3b, there were slight differences in both the initial $(ratio)_A$ and the sensitivities from the different mixing ratios. Both the sensitivity and the initial $(ratio)_A$ were highest in the case of the 1:1:1 (B:tA:tC) mixing ratio and decreased with any higher portion of the tA and tC strands. We are not certain about the reason behind these interesting results but one possibility is that at a high concentration, free tA and tC strands start to invade domain 2:2* in the folded structure of the

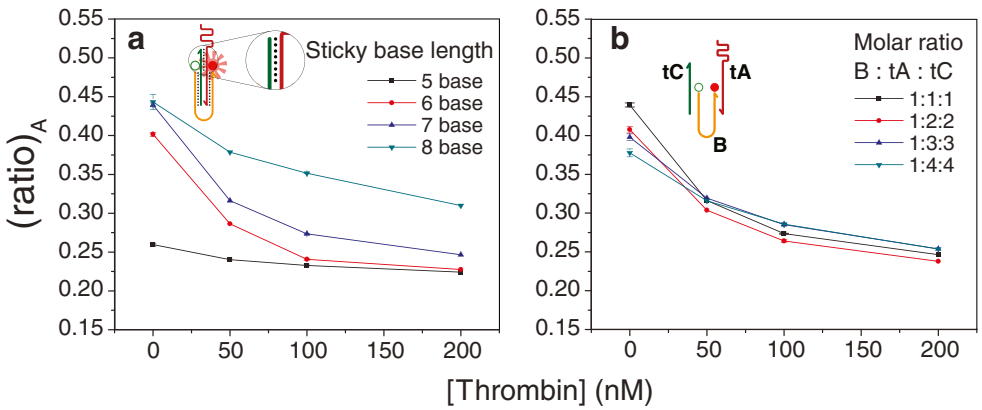

Fig. 3 **a** The effect of the sticky base length. The sticky base length was extended in the 3′ direction of the tC strand (in domain 2*), and the mixing ratio for all cases was 1:1:1 (B:tA:tC). **b** The effect of the strand mixing ratio. During the annealing process, the B strand was kept at 15 μM for all the mixing ratios and the tA and tC strands concentrations were varied according to the stated ratio. The sticky base length was 7. The working concentration of the sensors in all measurements were 133 nM based on the concentration of the B strand in 5 mM $MgCl_2$, 5 mM KCl and 1.77 mM NaCl in 10 mM Tris pH 8.0 containing 0.1 %w/v BSA. Three independent measurements were done at 0 and 100 nM of thrombin concentrations for every graph shown in (**a**) and (**b**) with the error bars indicating the standard deviation

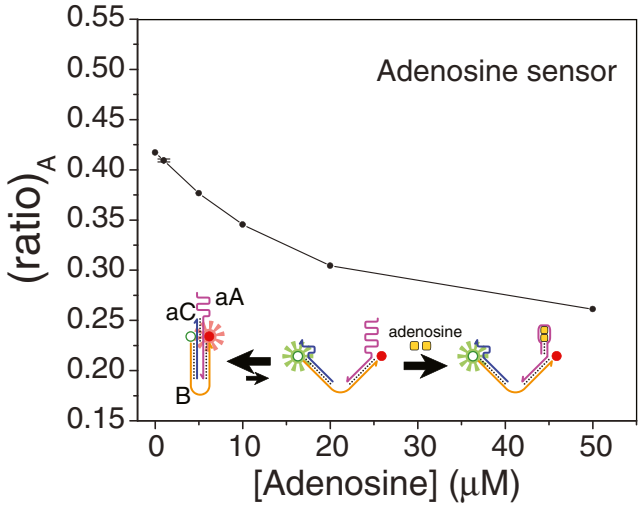

Fig. 4 Plot of the $(ratio)_A$ versus adenosine concentration showing a response from the adenosine sensor. The sensor was composed of the B strand doubly labeled with F and TMR. The aptamer strand and the complementary strand were an anti-adenosine aptamer and anti-an adenosine aptamer complementary (aA and aC strands). The decrease in the $(ratio)_A$ with increasing adenosine concentration resembled the case of the thrombin sensor with a linear detection range in the micro-molar region. The strand ratio of 1:1:1 (B:aA:aC) was used in the sensor preparation step and the sticky base length was 8. The working concentration of the sensor was 133 nM based on the concentration of the B strand in 5 mM $MgCl_2$, 5 mM KCl and 1.77 mM NaCl in 10 mM Tris pH 8.0 containing 0.1 %w/v BSA. Three independent measurements were done at 1 μM of adenosine concentration with the error bars indicating the standard deviation

annealed sensor, therefore, lowering the initial $(ratio)_A$. Since the $(ratio)_A$ at high concentration of thrombin should be comparable across all mixing ratios, decreasing the initial value also decreases the sensitivity. More experiments are needed to verify our hypothesis on the 2:2* domain being invaded at high tA/tC concentrations, and as far as the performance of the sensor is concerned, the mixing ratio of 1:1:1 (B:tA:tC) was used for later experiments.

Adenosine Sensor

To prove that the sensor design is not limited to only one aptamer-target partner, we chose adenosine as a second model target. Unlike thrombin, adenosine is a weak binding target with the dissociation constant in the micro-molar range [36]. The adenosine sensor has the same B strand used for the thrombin sensor but the aptamer strand and its complementary strand were switched to an anti-adenosine aptamer strand and an anti-adenosine aptamer complementary strand (aA and aC strands; Figs. 1 and 4). The same working principle was applied: the majority of the sensor was in the folded conformation via the hybridization of the sticky ends between the aA and aC strands (domain 6:6*, Fig. 1b) and the binding of adenosine disrupted the hybridization leading to the unfolded structure. A preliminary result in Fig. 4 showed that the adenosine sensor had a high initial $(ratio)_A$ of ~0.42 in the absence of adenosine and the $(ratio)_A$ decreased significantly with increasing adenosine concentration before slightly tapering off at a high concentration. This was as expected from the behavior of the sensor as we have seen in the case of the thrombin sensor. The linear concentration range was in the micro-molar region which also agrees well with other aptamer based adenosine sensors [16]. Therefore, the adenosine sensor followed the same working principle and the B strand can be shared between the two sensors. We anticipate that this concept can also be applied to many more types of aptamers.

Reconfiguration

Next, we performed a reconfiguration experiment to demonstrate that starting from the thrombin sensor, the variable domain, i.e. the tA and tC strands, could be washed and the adenosine sensor could be constructed by assembling the aA and aC strands on the B strand. The experiment was done at room temperature in six separate mixing steps starting from the annealed thrombin sensor (step #1), the washing of the variable part of the thrombin sensor (step#2 and #3), the assembling of the variable part of the adenosine sensor (step #4 and #5) and the binding of adenosine sensor and adenosine (step #6). After incubation, the samples were diluted and $(ratio)_A$ measurements were performed (see the Supplementary information for the mixing procedures). The results are shown in Fig. 5.

Next to each data point is a cartoon drawing, along with its name of an anticipated sensor form, an expected $(ratio)_A$ obtained from previous experiments (the first number in parentheses) and an actual $(ratio)_A$ measured in this experiment (the second number). In the mixing step #1 the measured $(ratio)_A$ of the annealed thrombin sensor was~0.43 as expected. The washing was done by adding the suitable complementary strands, the so called washers (tCW-4 and tAW-4, Fig. 1). In step#2 the tCW-4 washer was mixed with the annealed thrombin sensor at the molar ratio of 5:1 (tCW-4:sensor) to remove the tC strand while in step#3 the tCW-4 and the tAW-4 washers were added to remove both the tA and the tC strands from the thrombin sensor at the molar ratio of 5:5:1 (tCW-4:tAW-4:sensor). The single stranded overhang on the tA strand (domain 1 and 2 combined) and on the tC strand (domain 2*) served as a "toehold" [37] for the washers to bind before strand displacement by branch migration leaving the B strand bare. The negative free

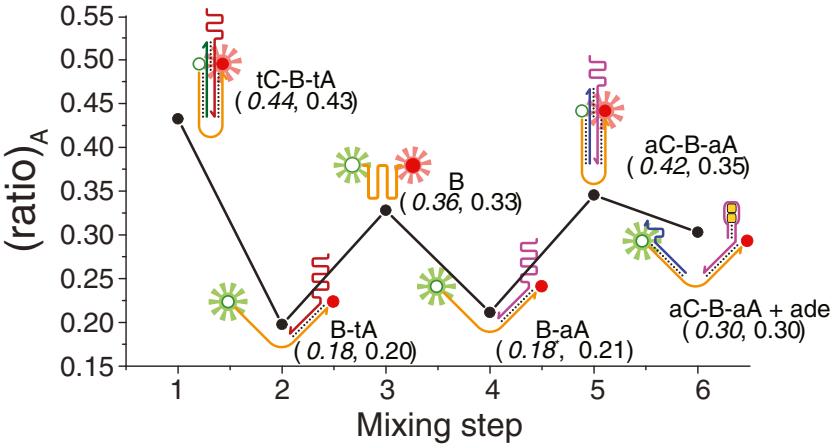

Fig. 5 Plot of the $(ratio)_A$ taken from different mixing steps of a reconfiguration experiment. For a given mixing step, the cartoon drawing next to each data point shows the expected form of the sensor along with its name, the expected $(ratio)_A$ (first number in parentheses) deduced from the results shown previously and the actual $(ratio)_A$ (second number) measured in this experiment. The expected $(ratio)_A$ of the mixing step #4 is assumed to be the same as that of the mixing step #2 due to structural similarity even though no prior measurement has been made. See the Supplementary information for the mixing procedures

energy changes calculated using UNAFold [21] ensures that the washing was favorable. Washing away the tC strand in step #2 made the $(ratio)_A$ drop to 0.20 and removing both the tC and tA strands in step #3 made it increase to 0.33; both are close to the values of 0.18 and 0.36 obtained from a separate set of measurements on samples prepared with the strand B annealed to the strand tA and on a sample with only the strand B present, respectively (see Figure 7 in the Supplementary information section).

In step #4, the aA strand assembly on the B strand (molar ratio of 2:1 aA:B) decreased $(ratio)_A$ to 0.21, which was still close to the expected value. The measured $(ratio)_A$ of ~0.35 after incorporating both the aA and aC strand on the B strand (molar ratio of 2:2:1 aA:aC:B) in step #5 was lower than the 0.42 obtained previously (the initial $(ratio)_A$ in Fig. 4). We believe that this was due to the fact that in this experiment the assembly was carried out at room temperature not at 90 °C as done previously. Therefore, there might still be some unwanted secondary structure hindering the annealing. Nevertheless the reconfigured sensor still responded to 20 μM adenosine as shown in step #6. Note that a perfect match between the expected and the actual $(ratio)_A$ in this step could be merely incidental. In summary, the results from the mixing step #1 to #4 agreed quite well with the expected values and in the mixing step #5 it was likely to have incomplete annealing. However, the sensor still behaved in the direction that we anticipated. Consequently, this experiment verified our claim that by dividing a molecular beacon aptamer into 2 parts, one type of sensor can be reconfigured to be another type by a simple washing —assembling of the variable domain while the expensive labeled constant domain is still in use. Even though the current version of our sensor, being free in bulk solution, has some limitations, such as some incomplete annealing or the wastes that keep piling up after each step of mixing, it has shown that our principles are correct. Some modifications, such as surface immobilization, should improve its performance. We believe that the design will be beneficial, for example, in an area of high throughput screening based on DNA chip technology. By immobilizing our sensor on the surface, the chip design and construction will be more flexible and can be reconfigured to detect multiple targets.

Conclusion

In this study, we have demonstrated that a reconfigurable molecular aptamer beacon was possible to construct and the structural changes of the sensor can be followed by the $(ratio)_A$ method. By dividing the sensor into two modules, the expensive labeled part was static, and is shared while the anti-target aptamer part was labile and can be replaced at low cost. We chose to construct a thrombin sensor and an adenosine sensor using this concept and the detection ranges were comparable to conventional molecular aptamer beacons. Once created, the thrombin sensor can be reconfigured to be an adenosine sensor by the help of proper washers. Though there is some room for improvements on the efficiency of reconfiguring, we believe that with some modifications, such as surface immobilization, we can improve this prototype further to be used in an area of high throughput detections based on DNA chip technology where various types and large amounts of molecular aptamer beacons are immobilized for detection of multiple targets.

Acknowledgements We would like to acknowledge the financial support from the Thailand Research Fund and the Office of Higher Education Commission (MRG5280160). The financial and instrumental supports from the Trace Analysis and Biosensor Research Center, from the Department of Physics and from the Department of Chemistry, Faculty of Science, Prince of Songkla University are highly appreciated. We also thank Dr. Chongdee Thammakhet for useful discussions and Dr. Brian Hodgson for his help in a proof reading of the manuscript.

References

1. Cho EJ, Lee JW, Ellington AD (2009) Applications of Aptamers as Sensors. In: Annual Review of Analytical Chemistry, vol 2. Annual Review of Analytical Chemistry. Annual Reviews, Palo Alto, pp 241–264. doi:10.1146/annurev.anchem.1.031207.112851
2. Ellington AD, Szostak JW (1990) *In vitro* selection of RNA molecules that bind specific ligands. Nature 346:818–822
3. Tuerk C, Gold L (1990) Systematic evolution of ligands by exponential enrichment—RNA ligands to bacteriophage-T4 DNA-polymerase. Science 249(4968):505–510
4. Jayasena SD (1999) Aptamers: An emerging class of molecules that rival antibodies in diagnostics. Clin Chem 45(9):1628–1650
5. Xiao Y, Lubin AA, Heeger AJ, Plaxco KW (2005) Label-free electronic detection of thrombin in blood serum by using an aptamer-based sensor. Angew Chem Int Ed 44(34):5456–5459
6. Liss M, Petersen B, Wolf H, Prohaska E (2002) An aptamer-based quartz crystal protein biosensor. Anal Chem 74(17):4488–4495. doi:10.1021/ac011294p
7. Gebhardt K, Shokraei A, Babaie E, Lindqvist BH (2000) RNA Aptamers to S-Adenosylhomocysteine: kinetic properties, divalent cation dependency, and comparison with anti-S-adenosylhomocysteine antibody. Biochemistry 39(24):7255–7265. doi:10.1021/bi000295t
8. Pavlov V, Xiao Y, Shlyahovsky B, Willner I (2004) Aptamer-functionalized Au nanoparticles for the amplified optical detection of thrombin. J Am Chem Soc 126(38):11768–11769. doi:10.1021/ja046970u
9. Hermann T, Patel DJ (2000) Adaptive recognition by nucleic acid aptamers. Science 287(5454):820–825
10. Potyrailo RA, Conrad RC, Ellington AD, Hieftje GM (1998) Adapting selected nucleic acid ligands (aptamers) to biosensors. Anal Chem 70(16):3419–3425
11. Hamaguchi N, Ellington A, Stanton M (2001) Aptamer beacons for the direct detection of proteins. Anal Biochem 294(2):126–131
12. Stojanovic MN, de Prada P, Landry DW (2000) Fluorescent sensors based on aptamer self-assembly. J Am Chem Soc 122:11547–11548
13. Tyagi S, Kramer FR (1996) Molecular beacons: trobes that fluoresce upon hybridization. Nat Biotechnol 14(3):303–308. doi:10.1038/nbt0396-303
14. Tyagi S, Bratu DP, Kramer FR (1998) Multicolor molecular beacons for allele discrimination. Nat Biotechnol 16(1):49–53. doi:10.1038/nbt0198-49
15. Li JJ, Fang X, Tan W (2002) Molecular aptamer beacons for real-time protein recognition. Biochem Biophys Res Commun 292:31–40
16. Nutiu R, Li Y (2003) Structure-switching signaling aptamers. J Am Chem Soc 125:4771–4778
17. Stojanovic MN, Landry DW (2002) Aptamer-based colorimetric probe for cocaine. J Am Chem Soc 124(33):9678–9679. doi:10.1021/ja0259483
18. Xu WC, Lu Y (2010) Label-free fluorescent aptamer sensor based on regulation of malachite green fluorescence. Anal Chem 82 (2):574–578. doi:10.1021/ac9018473
19. Zhang DY, Seelig G (2011) Dynamic DNA nanotechnology using strand-displacement reactions. Nat Chem 3:103–113
20. Bock LC, Griffin LC, Latham JA, Vermaas EH, Toole JJ (1992) Selection of single-stranded DNA molecules that bind and inhibit human thrombin. Nature 355:564–566
21. Markham NR, Zuker M (2008) UNAFold: software for nucleic acid folding and hybridization. Methods Mol Biol 453:3–31
22. Volkin E, Cohn WE (1954) Estimation of nucleic acids. Methods Biochem Anal 1(304):287–305
23. Clegg RM, Murchie AIH, Zechel A, Carlberg C, Diekmann S, Lilley DMJ (1992) Fluorescence resonance energy-transfer analysis of the structure of the 4-Way DNA junction. Biochemistry 31 (20):4846–4856
24. Clegg RM (1992) Fluorescence resonance energy transfer and nucleic acids. Methods Enzymol 211:353–388
25. Majumdar ZK, Hickerson R, Noller HF, Clegg RM (2005) Measurements of internal distance changes of the 30 S ribosome using FRET with multiple donor-acceptor pairs: quantitative spectroscopic methods. J Mol Biol 351:1123–1145
26. Lakowicz JR (1999) Principles of fluorescence spectroscopy, 2nd edn. Kluwer Academic/Plenum Publishers, New York
27. Williamson JR, Raghuraman MK, Cech TR (1989) Monovalent cation-induced structure of telomeric DNA: the G-quartet model. Cell 59(5):871–880
28. Acevedo OL, Dickinson LA, Macke TJ, Thomas CAJ (1991) The coherence of synthetic telomeres. Nucleic Acids Res 19:3409–3419
29. Williamson JR (1994) G-quartet structures in telomeric DNA. Annu Rev Biophys Biomol Struct 23:703–730
30. Wang KY, McCurdy S, Shea RG, Swaminathan S, Bolton PH (1993) A DNA Aptamer Which Binds to and Inhibits Thrombin Exhibits a New Structural Motif for DNA. Biochemistry 32 (8):1899–1904
31. Wang KY, Krawczyk SH, Bischofberger N, Swaminathan S, Bolton PH (1993) The tertiary structure of a DNA aptamer which binds to and inhibits thrombin determines activity. Biochemistry 32(42):11285–11292
32. Bloomfield VA, Crothers DM, Tinoco IJ (2000) Nucleic acids: structures, properties, and functions. University Science, Sausalito
33. He F, Tang Y, Wang S, Li Y, Zhu D (2005) Fluorescent amplifying recognition for DNA G-quadruplex folding with a cationic conjugated polymer: a platform for homogeneous potassium detection. J Am Chem Soc 127(35):12343–12346. doi:10.1021/ja051507i
34. Nagatoishi S, Nojima T, Galezowska E, Gluszynska A, Juskowiak B, Takenaka S (2007) Fluorescence energy transfer probes based on the guanine quadruplex formation for the fluorometric detection of potassium ion. Anal Chim Acta 581:125–131
35. Padmanabhan K, Padmanabhan KP, Ferrara JD, Sadler JE, Tulinsky A (1993) The structure of α-thrombin inhibited by a 15-mer single-stranded DNA aptamer. J Biol Chem 268(24):17651–17654
36. Huizenga DE, Szostak JW (1995) A DNA aptamer that binds adenosine and ATP. Biochemistry 34:656–665
37. Yurke B, Turberfield AJ, Mills AP, Simmel FC, Neumann JL (2000) A DNA-fuelled molecular machine made of DNA. Nature 406(6796):605–608